Austrian Journal of Earth Sciences | Vienna | 2024 | Volume 117 | 73–86 | DOI: 10.17738/ajes.2024.0006

Raman Spectroscopy of carbonaceous material thermometry in the Carnic Alps (Austria, Italy)

Gerd Rantitsch[1*]

[1)] Montanuniversität Leoben, Chair of Geology and Economic Geology, 8700 Leoben, Austria

[*)] Corresponding author: gerd.rantitsch@unileoben.ac.at

Keywords: Carnic Alps, Southern Alps, Metamorphism, Raman Spectroscopy of carbonaceous material

Abstract

The Carnic Alps (eastern Southern Alps) provide a classical area to study polyphase very-low- to low-grade metamorphism within the Variscan belt of Europe. Temperature indicators collected during the past three decades map the general metamorphic structure of a mountain chain affected by three major tectonic events (Variscan and Alpine thrusting, Oligocene transpression). Thermometric data obtained by Raman Spectroscopy of carbonaceous material (RSCM) described in this study extend the already published database, provide a map of metamorphic isotherms, and are interpreted in the view of current tectonic concepts. The RSCM temperatures of this study describe a gradient between ca. 460 °C in the tectonically deepest segments, bordered by the Periadriatic Fault System, and temperatures of ca. 200 °C in Permian-Triassic boundary strata of the Gartnerkofel-1 core. Mapped isotherms indicate three domains with different thermal histories, characterized by Variscan imbrication of an accretionary wedge, Permo-Mesozoic burial, and Oligocene contact metamorphism.

1. Introduction

The Carnic Alps (Fig. 1) exposes an extraordinary record of the sedimentary and paleontological heritage of the Variscan (Pennsylvanian) orogeny (Schönlaub and Heinisch, 1993; Schönlaub and Histon, 2000; Corradini and Suttner, 2015) at the southern margin of the European Variscides (e.g., Mariotto and Venturini, 2019; Neubauer et al., 2022). Following the post-orogenic molasse phase, the Variscan chain of the Carnic Alps drowned (Schönlaub and Forke, 2007), und became later also a segment of the Mesozoic to Cenozoic Alpine chain (Mariotto and Venturini, 2019), dissected subsequently during Miocene-Pliocene strike-slip tectonics along the Periadriatic Fault System (Fodor et al., 1998; Frisch et al., 1998, 2000; Mancktelow et al., 2001; Bartel et al., 2014; Heberer et al., 2017; Klotz et al., 2019). Due to excellent exposures and an extraordinarily rich fossil content, the Carnic Alps represents a key area to understand Paleozoic life and provides a natural laboratory to study orogenic processes. Geoscience data were collected since 1824 (Schönlaub and Forke, 2023), providing now a complete geological map coverage (Schönlaub, 1985b, 1987, 1989, 1997, 2007; Hubich et al., 2000; Venturini et al., 2001; Pondrelli et al., 2020), a comprehensive stratigraphical database (Schönlaub and Forke, 2007; Corradini and Suttner, 2015; Pondrelli et al., 2020), modern tectonic models (Läufer et al., 1997, 2001; Hubich et al., 2000; Schönlaub and Forke, 2007; Mariotto and Venturini, 2019 cum. lit.; Curzi et al., 2024), as well as metamorphic (Sassi et al., 1995; Läufer et al., 1997; Rantitsch, 1997; Hubich et al., 2000; Sassi et al., 2004; Brime et al., 2008), and thermochronological (Dallmeyer and Neubauer, 1994; Läufer, 1996; Läufer et al., 1997; Meli, 2004; Mader et al., 2007) data.

The Variscan and Alpine orogenic cycles left a very-low grade to low grade metamorphic imprint of similar grade (Rantitsch, 1997; Rainer et al., 2009), which challenges the reconstruction of the thermo-tectonic history. Important information derives from mapped metamorphic indicators including Kübler Index (KI, i.e. "illite crystallinity") data (Árkai et al., 1991; Schramm, 1991; Schönlaub et al., 1992; Árkai et al., 1995; Sassi et al., 1995; Läufer et al., 1997; Rantitsch, 1997; Hubich et al., 2000; Nussbaum, 2000; Brime et al., 2008), fluid inclusion data (Rantitsch, 1997),

graptolite and vitrinite reflectance data (Rantitsch, 1992; Sassi et al., 1995; Rantitsch, 1995b, 1997; Rantitsch et al., 2000; Rainer and Rantitsch, 2002; Rantitsch, 2007), and Conodont Alteration indices (CAI, Pondrelli, 2002; Brime et al., 2008). KI brackets the field of very-low grade metamorphism (defining the "anchizone" between the zone of diagenesis and the low-grade metamorphic "epizone") in pelitic rocks (e.g., Árkai et al., 2004; Ferreiro Mählmann et al., 2012; Warr and Ferreiro Mählmann, 2015), but is influenced by strain and the heat flow history of the investigated sample (Ferreiro Mählmann et al., 2012). CAI data are valuable to assess the metamorphic grade of Paleozoic to Triassic carbonate rocks (Epstein et al., 1977; Rejebian et al., 1987), but they are not very sensitive to rising metamorphic temperatures in some instances (McMillan and Golding, 2019). Vitrinite reflectance data (e.g., Pusz et al., 2014) lose their thermometrical sensitivity above ca. 250°C (Rantitsch et al., 2020 a). Thus, despite a good data coverage, there is certain demand to improve the present view of metamorphism in the Carnic Alps by the use of Raman spectroscopy of carbonaceous material (RSCM), estimating metamorphic temperatures without reference to kinetic parameters and assumed boundary conditions, as needed e.g., to convert vitrinite reflectance data to burial temperatures.

RSCM (reviewed by Henry et al., 2019) provides a well-established method to investigate a polymetamorphic unit to confidently estimate peak metamorphic temperatures (e.g., Rantitsch et al., 2020a; Rantitsch, 2023). The RSCM calibration used in this study (Lünsdorf et al., 2017) spans the temperature range that overprinted the pre-Variscan basement and post-Variscan cover units of the Carnic Alps. Therefore, the goal of this study is to use RSCM data to map metamorphic peak temperature isograds. Based on a review of the current state of knowledge, it is attempted to give a better view on the metamorphic structure of the Carnic Alps.

2. Geological setting

The northeastern edge of the Southalpine unit (Carnic Domain of Neubauer et al., 2022) was uplifted along the Periadriatic Fault System during Miocene to Pliocene times (Vrabec and Fodor, 2006; Heberer et al., 2017; Klotz et al., 2019). As a result, Variscan (Ordovician to Pennsylvanian) basement units, overlain by Pennsylvanian to Triassic cover sequences, were exhumed in the Carnic Alps, in the Jesenice Rise, and in the South-Karawanken Rise (Fig. 1). During pre-Mesozoic times, they belonged together with adjacent Austroalpine units (Noric Domain of Neubauer et al., 2022) to a continental block (Paleo-Adria of Neubauer et al., 2022) between northern Gondwana and Baltica (Ebner et al., 2008; Haas et al., 2020; Neubauer et al., 2022), which collided with external Variscan units due to the closure of an oceanic domain during the Pennsylvanian Variscan orogeny (Neubauer et al., 2022, cum. lit.). Later, the Carnic Alps were also involved in the Cretaceous to Cenozoic Alpine orogeny (e.g., Schmid et al., 2004).

The Carnic Alps are separated by the Pustertal-Gailtal-Fault, a segment of the Periadriatic Fault System, from the northerly adjacent Austroalpine unit (Figs. 1, 2). Along the fault trace, ductily deformed Southalpine schists and limestones (Eder Nappe of Schönlaub, 1985b, 1987, 1989; Eder and Mauthner Klamm Units of Läufer et al., 1997; Fig. 2), related to burial under low-grade metamorphic conditions and Oligocene shearing, were exhumed transpressionally during Mid-Miocene times (Läufer et al., 1997).

Lithostratigraphically, the presence of Visean to Bashkirian flysch sediments below a Late Bashkirian to Moscovian angular discordance, groups the mapped formations into a pre-Variscan (Middle Ordovician to Visean), a syn-Variscan (Visean to Bashkirian), and a post-Variscan (Kasimovian to Triassic) sequence (Schönlaub and Heinisch, 1993; Schönlaub and Forke, 2007; Corradini and Suttner, 2015). Ordovician metasediments, carbonates and acidic volcanics of a back-arc (Siegesmund et al., 2023) or rift (Neubauer et al., 2022) basin at the northern Gondwana margin were overlain in the Silurian by sediments of a shallow- to deep-marine realm (Schönlaub and Histon, 2000; Pondrelli et al., 2020). Subsequently, thick Devonian to Lower Mississippian platform carbonates and sediments of adjacent pelagic basins (Schönlaub and Histon, 2000; Pondrelli et al., 2020) were deposited at the pre-Variscan stage. A Variscan active margin (Schönlaub and Histon, 2000; Läufer et al., 2001) is indicated by Upper Visean to Late Bashkirian flysch sediments (Hochwipfel Formation, e.g., Krainer, 1992). The post-Variscan stage started with Kasimovian to Gzhelian molasse sediments of a mixed terrestrial to shallow marine regime (Auernig Formation, e.g., Krainer, 1992), which evolved to Sakmarian to Artinskian platform carbonates (Schönlaub and Forke, 2007). After a phase of strong block faulting in the Late Cisuralian, westward transgression of the Tethyan ocean resulted in the deposition of Early Triassic fast-growing carbonate platforms, which evolved to a well-developed rimmed platform in the Norian to Rhaetian (Schönlaub and Forke, 2007).

According to Läufer et al. (1993), Kullmann and Loeschke (1994), Hubich et al. (2000) and Läufer et al. (2001), the backbone of the Carnic Alps constitutes a south-vergent Late Devonian to Pennsylvanian accretionary wedge, composed of syn-orogenic flysch sediments (Hochwipfel Formation), imbricated with huge olistoliths, outcropping in the Hochwipfel Nappe (Hubich et al., 2000; Läufer et al., 2001; Fig. 2). Structural subunits were formerly interpreted as nappes (Schönlaub, 1985a) and mapped along the central and eastern chain (Schönlaub, 1985b, 1987, 1989, 1997). Thus, nappe-sections can be correlated over wide distances.

The Hochwipfel Nappe was overridden by the Cellon-Kellerwand Nappe (Schönlaub, 1985a; Läufer et al., 2001; Fig. 2), which exposes along several complete sections Late Ordovician clastic sediments and carbonates, Silurian deep-water sediments and Devonian to Mississippian platform carbonates in a widely segmented facies structure (Schönlaub and Forke, 2007; Corradini and

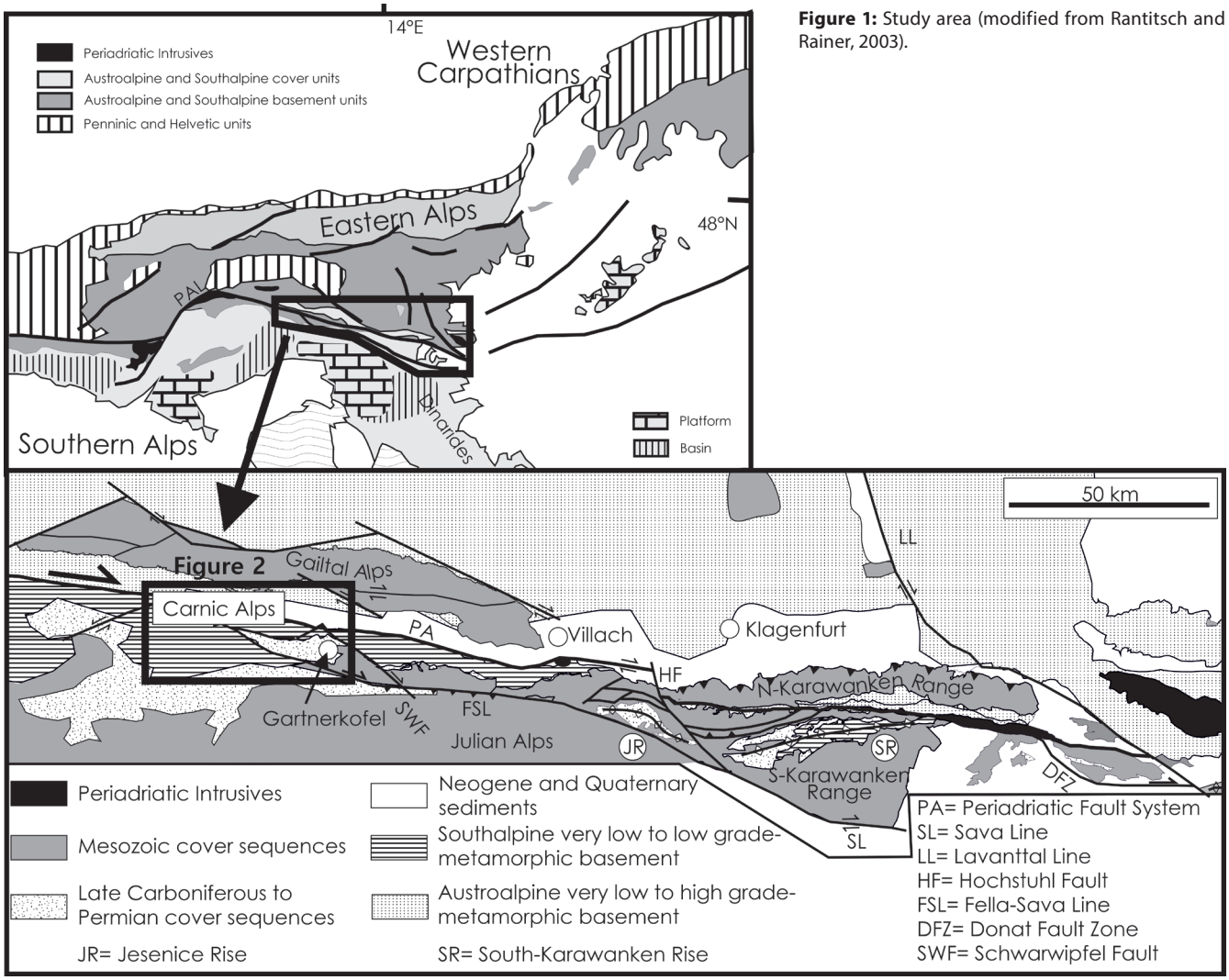

Figure 1: Study area (modified from Rantitsch and Rainer, 2003).

Suttner, 2015; Pondrelli et al., 2020). Mississippian flysch sediments cover this sequence (Schönlaub, 1985b, 1987, 1989, 1997, 2007; Hubich et al., 2000; Venturini et al., 2001; Pondrelli et al., 2020). In the model of Läufer et al. (2001), the overthrusting Cellon-Kellerwand Nappe sourced syn-tectonically the olistoliths of the tectonically lower accretionary wedge towards the south. However, Mariotto and Venturini (2019, cum. lit.), favored a model of syn-sedimentary tectonics attributed to a Devonian to Mississippian wrench corridor and SSW-directed folding and imbrication during the Pennsylvanian.

The tectonically highest Fleons Nappe (Fig. 2) covers the entire western Carnic Alps (Hubich et al., 2000; Läufer et al., 2001; Mariotto and Venturini, 2019). It comprises Upper Ordovician metasediments and metavolcanics, Silurian deep-water sediments, Devonian limestones and presumably Mississippian flysch sediments (Läufer et al., 2001), thrusted along the Val Bordaglia fault above the Cellon-Kellerwand Nappe (Hubich et al., 2000; Läufer et al., 2001; Mariotto and Venturini, 2019). Post-Variscan strata overlie the nappe stack unconformably and give evidence of the Variscan age of nappe stacking (Hubich et al., 2000; Läufer et al., 2001, Venturini et al., 2001; Schönlaub and Forke, 2007; Mariotto and Venturini, 2019).

Alpine (Eocene to Pliocene) tectonics shaped a south-vergent thrust-and-fold wedge, uplifted along a Miocene ramp-flat structure (Castellarin and Cantelli, 2000; Mariotto and Venturini, 2019). Activity of the related Valsugana Thrust is dated back to the Late Cretaceous (Curzi et al., 2024). Therefore, top to the south deformation may have started earlier. Pre-existing (Variscan) structures were largely overprinted, however, large Variscan folds in the Cellon-Kellerwand Nappe remained preserved (Mariotto and Venturini, 2019).

The thermal imprint of the eastern and central Carnic Alps (east of the Val Bordaglia Fault) reached greenschist facies conditions in the Eder and Mautner Klamm Units and diagenetic conditions in Permian-Triassic boundary strata of the post-Variscan overburden (Schramm, 1991; Schönlaub et al., 1992; Läufer, 1996; Rantitsch, 1997; Läufer et al., 1997; Rainer and Rantitsch, 2002). The entire Hochwipfel Nappe in-between underwent very-low grade metamorphism, described by a continuous bottom-to-top decrease of the metamorphic rank and WNW-

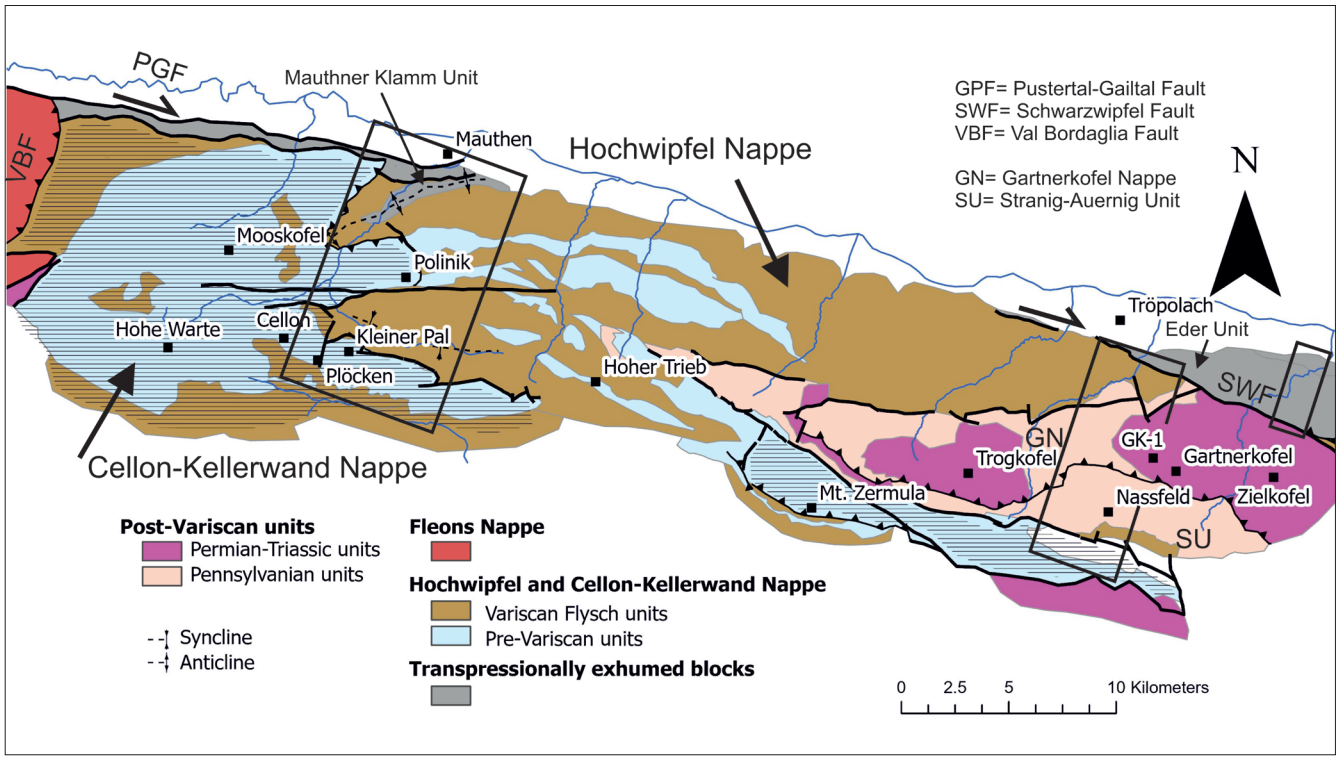

Figure 2: Simplified geological map of the Carnic Alps (redrawn from Schönlaub, 1985b, 1987, 1989, 1997, 2007; Hubich et al., 2000; Venturini et al., 2001; Pondrelli et al., 2020). Note that the Variscan thrust between the Hochwipfel Nappe and the Cellon-Kellerwand Nappe (shaded, Läufer et al., 2001) is widely dissected by post-Variscan faults. The frames indicate two sampled sections (Mauthen Section in the West, Nassfeld Section in the East). Permian-Triassic boundary sediments from the Gartnerkofel-1 (GK-1) core were investigated near to the Gartnerkofel peak.

ESE orogen-parallel oriented isograds (Rantitsch, 1997). No metamorphic hiatus occurs at the Variscan unconformity (Rantitsch, 1997). Here, $^{40}Ar/^{39}Ar$ data of post-Variscan detrital white mica evidence a very weak Variscan tectonothermal effect on deeply buried and rapidly exhumed source rocks, which were also not significantly overprinted (at temperatures below 250–300 °C) during later times (Dallmeyer and Neubauer, 1994; Mader et al., 2007). Clay mineralogical evidence points to a high heat-flow during deposition of the post-Variscan molasse sediments (Rantitsch, 1997). The low extent of the Alpine overprint is constrained by kinetic modelling of vitrinite reflectance data, indicating that Carboniferous to Mesozoic sedimentary burial explains the organic maturity of Carboniferous strata of the Carnic Alps (Rantitsch, 1997), other segments of the Southern Alps (Rantitsch and Rainer, 2003), Dinarides (Rainer et al., 2009, 2016), and formerly adjacent Austroalpine units (Rantitsch, 1995a; Rantitsch et al., 2020).

The Fleons Nappe of the western Carnic Alps was metamorphosed under greenschist facies conditions (Árkai et al., 1991; Sassi et al., 1995; Hubich et al., 2000; Läufer et al., 2001; Sassi et al., 1995, 2004) by a penetrative Variscan (Läufer, 1996; Läufer et al., 2001; Meli, 2004) imprint, increasing continuously towards the west (Meli et al., 2004 cum. lit.).

3. Samples

As the northern slope of the Carnic Alps exposes complete sections through the nappe-stack, metapelites were sampled here from two cross-sections and also from some isolated localities in-between (Fig. 2, Tab. 1). CAI data of Brime et al. (2008) are used to trace the metamorphic imprint in metapelite-free carbonate units. According to the given nappe architecture (see above), the sections are correlated in respect to their nappe-stack positions by using the structural names of Schönlaub (1985a) as names of individual units of the Hochwipfel Nappe (Mauthneralm Unit, Feldkogel Unit, Rauchkofel Imbricate Unit, Bischofalm Unit from bottom to top, Fig. 3).

The Mauthen Section (Figs. 2, 3 a) cuts the entire nappe-stack of the Carnic Alps (Schönlaub, 1985a, b). An imbricated segment of the Mauthner Klamm Unit (Läufer et al., 1997) with epizonal KI values (Läufer, 1996; Rantitsch, 1997; Brime et al., 2008), a CAI of 5½ – 6 (Brime et al., 2008), and graphitic carbonaceous matter (Rantitsch, 1997) is sampled at the bottom. Tectonically above, the structural base units of the Hochwipfel Nappe were sampled in an anticline and within the overlying Cellon-Kellerwand Nappe with CAI values between 5½ and 7½ (Brime et al., 2008). The carbonates of the Feldkogel Unit show CAI values of 5 – 5½ (Brime et al., 2008). Tectonically upward, the CAI values decrease to 4 – 4½ and KI values in-

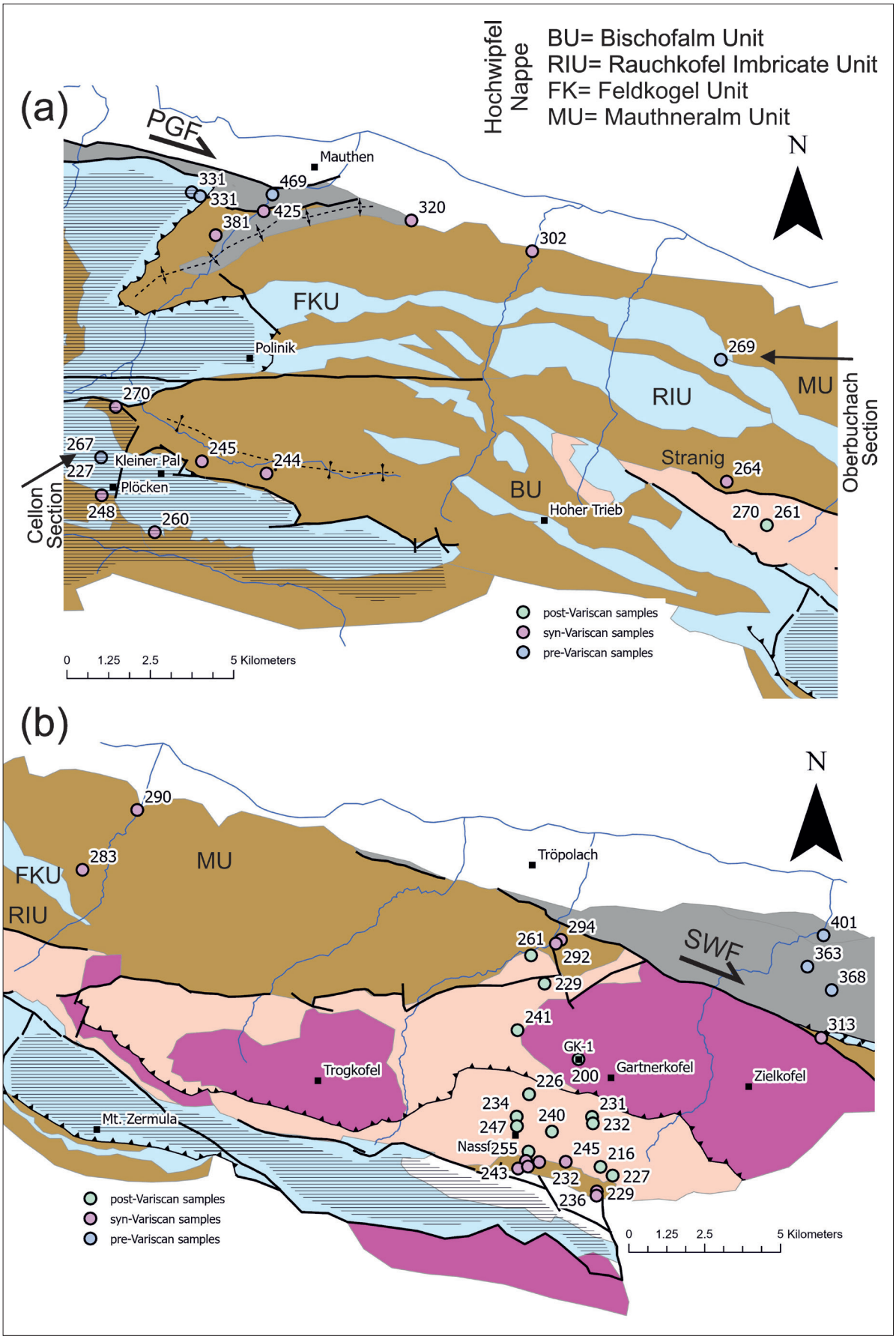

Figure 3: RSCM maximum temperatures (°C) in the Carnic Alps (legend in Fig. 2). The Hochwipfel Nappe units (Schönlaub, 1985a) are labeled in the map.

dicate the anchizone (Brime et al., 2008). In this segment, graptolite shales of the Oberbuchach Section (Jaeger and Schönlaub, 1980) were sampled in the overlying Rauchkofel Imbricate Unit, yielding graptolite reflectance values between 5.0 and 8.6 %Rmax and anchizonal KI values, decreasing to the top (Rantitsch, 1997). At the top of the Hochwipfel Nappe, the Bischofalm Unit and the post-Variscan Auernig Formation were sampled. Vitrinite reflectance values vary between 2.8 and 5.0 %Rmax (Rantitsch, 1997). KI data indicate the lower part of the Anchizone (Rantitsch, 1997). The topmost Cellon-Kellerwand Nappe was sampled in the Cellon Section of the Plöcken area (Corradini et al., 2015) and in conformably overlying (Pondrelli et al., 2020) flysch sediments.

The eastern Nassfeld Section (Figs. 2, 3b) exposes the epizonal (Läufer, 1996; Läufer et al., 1997; Rantitsch, 1997) Eder Unit at the base. Carbonate rocks contain conodonts with CAI 5½ – 6 (Brime et al., 2008). Intercalated metapelites contain graphitic carbonaceous matter (Rantitsch, 1997). The overlying Mauthneralm Unit of the Hochwipfel Nappe was sampled on both sides of the dextral Schwarzwipfel strike-slip fault (Fig. 3b), related to the transpressional Miocene exhumation of the Eder Unit (Läufer et al., 1997; Forke et al., 2008). Further samples come from the overlying post-Variscan Auernig Formation, exposed in the autochtonous Stranig-Auernig Unit and tectonically above in the Gartnerkofel Nappe (Schönlaub and Forke, 2007). Vitrinite reflectance ranges between 2.0 and 3.0 %Rmax (Rantitsch, 1997), and KI values indicates anchizonal conditions (Läufer, 1996; Rantitsch, 1997). Upper Permian to Lower Triassic pelitic beds of the Gartnerkofel-1 core (Fig. 2; Holser et al., 1989; Holser and Schönlaub, 1991) were investigated as well. In the sampled interval, vitrinite reflectance varies between 1.4 and 2.2 %Ro (Rainer and Rantitsch, 2002) and KI values indicate diagenetic conditions (Schramm, 1991). In the Stranig-Auernig Unit, the sedimentary contact between Hochwipfel and Auernig Formations (Schönlaub, 2007) was sampled in both formations. Vitrinite reflectance data of the upper part of the section are described in Rantitsch (2007). Carbonates of the Cellon-Kellerwand Nappe contain conodonts with a CAI of 3–4 (Brime et al., 2008).

4. Methods

Raman spectroscopy of carbonaceous material (RSCM) investigates the interaction of laser light with carbonaceous material (CM) in inelastic scattering giving a spectrum, which assesses the state of structural order (see Lünsdorf, 2016 for a review). The CM order is related irreversibly to peak metamorphic temperatures (see Henry et al., 2019 for a review). CM from the metasediments of this study was concentrated by an acid (HCl and HF) treatment of crushed sample material. A Horiba Labram HR Evolution instrument, equipped with a 100 mW Nd:Yag (532 nm) laser, a confocal microscope (100x objective with a 0.80 numerical aperture and a confocal hole aperture of 100 µm), a 1800 g/mm grating, and a Peltier cooled CCD detector was used to collect Raman spectra. Filters to minimize the output laser power to < 1mW were used to avoid any sample damage. The wavenumbers were calibrated with the Rayleigh scattering (0 cm^{-1}), and a silicon wafer (520.7 cm^{-1}). 20 spectra per sample over the 700–2000 cm^{-1} spectral region were collected, evaluated by the IFORS software of Lünsdorf and Lünsdorf (2016), which excludes subjectivity in curve-fitting (Lünsdorf et al., 2014), and characterized by median spectral parameters of Lünsdorf et al. (2017). In particular, the D-STA parameter (total area, scaled by the maximum intensity in the D-band region) reliably describes the evolution of dispersed organic matter during coalification and graphitization (Lünsdorf, 2016; Lünsdorf and Lünsdorf 2016; Lünsdorf et al., 2017). Metamorphic peak temperatures were calculated from a calibration function established by spectral data collected on standard samples (Lünsdorf et al., 2017), as described above. It is important to note that the given uncertainty of the temperature estimates of 25–30 °C (Tab. 1) is controlled primary by the uncertainty of the (petrologically determined) uncertainty of the used calibration sample set (Lünsdorf et al., 2017). The calculated spectral parameters show a higher within-sample precision of <10 % of the medians, yielding an outcrop precision of the median temperatures of ca. ± 10 °C (Tab. 1).

5. Results

In the Mauthen Section, metapelites from a separated slice of the Mauthner Klamm Unit (Fig. 3a, Tab. 1) yield a peak temperature of 469 °C. Ductily sheared limestones of the lowest structural unit of the Hochwipfel Nappe are imbricated in flysch sediments of the Hochwipfel Formation. A flysch sample near the contact indicates a metamorphic temperature of 425 °C. Tectonically upward, 381 °C is estimated. Two samples at a higher tectonic position show consistent temperatures of 331 °C, demonstrating an upright metamorphic trend without break in-between. Further to the east, the deepest flysch sediments are metamorphosed to ca. 300 °C. In a higher structural level, a graptolite schist sample from the Oberbuchach Section (Jaeger and Schönlaub, 1980; Rantitsch, 1992, 1995b) yields 269 °C. At the top of the Hochwipfel Nappe, the metamorphic temperature at the Variscan unconformity in the Stranig area is estimated with ca. 260–270 °C (Fig. 3a). Flysch samples at the top show 270 to 244 °C. In the Cellon Section of the Cellon-Kellerwand Nappe (Fig. 3a), RSCM temperature decrease continuously from 267 °C in the Upper Ordovician Uqua Formation to 227 °C in the Lochkovian Rauchkofel Formation (Tab. 1). Stratigraphically overlying flysch samples show 248 and 260 °C.

At the base of the Nassfeld Section (Fig. 3b, Tab. 1), the Eder Unit was metamorphosed at 400 °C. Paleotemperatures decrease to the top and reach 313 °C in the overlying Hochwipfel Nappe. At the western side of the

Sample	Formation		UTM33-E	UTM33-N	Z	Temp [°C]	+/-
Nassfeld Section							
GR23-16	Schist	Eder Unit	374914	5162093	670	401	28
GR23-15	Schist	Eder Unit	374536	5161394	1189	363	28
GR23-14	Schist	Eder Unit	375076	5160851	1318	368	28
GR23-13	Hochwipfel Fm	Mauthneralm Unit	374813	5159779	1507	313	27
GR1906	Hochwipfel Fm	Mauthneralm Unit	368954	5162117	795	294	27
GR23-17	Hochwipfel Fm	Mauthneralm Unit	368835	5162042	762	292	27
GR1806	Auernig Fm	Stranig-Auernig Unit	368267	5161786	917	261	27
GR17-06	Auernig Fm	Gartnerkofel Nappe	368558	5161135	1100	229	28
GR16-06	Auernig Fm	Gartnerkofel Nappe	367922	5160098	1223	241	28
GR1406	Auernig Fm	Stranig-Auernig Unit	367860	5158145	1494	234	28
GR1206	Auernig Fm	Stranig-Auernig Unit	368653	5157788	1740	240	27
GR13-06	Auernig Fm	Stranig-Auernig Unit	367861	5157925	1530	247	27
GR10-06	Auernig Fm	Stranig-Auernig Unit	369574	5158099	1838	231	28
GR0906	Auernig Fm	Stranig-Auernig Unit	369586	5157948	1900	232	29
NF10-21/5	Auernig Fm	Stranig-Auernig Unit	369739	5156963	1630	216	28
NF11-20/1	Auernig Fm	Stranig-Auernig Unit	370010	5156757	1530	227	28
NF6	Auernig Fm	Stranig-Auernig Unit	368114	5157341	1530	218	28
GR15-06	Auernig Fm	Stranig-Auernig Unit	368151	5158644	1395	226	28
NF9A-10/9	Hochwipfel Fm	Stranig-Auernig Unit	368952	5157095	1580	245	27
NF9B-17/3	Hochwipfel Fm	Stranig-Auernig Unit				232	28
NF8-22	Hochwipfel Fm	Stranig-Auernig Unit	368353	5157102	1600	246	27
NF5	Hochwipfel Fm	Stranig-Auernig Unit	368051	5157137	1400	255	27
NF3	Hochwipfel Fm	Stranig-Auernig Unit	367869	5156963	1350	243	27
NF2	Hochwipfel Fm	Stranig-Auernig Unit	369643	5156408	1320	229	28
NF1-24/23	Hochwipfel Fm	Stranig-Auernig Unit	369636	5156315	1300	236	31
NF4	Hochwipfel Fm	Stranig-Auernig Unit	368092	5157002	1350	235	27
Central samples							
GR23-18	Hochwipfel Fm		348911	5168486	705	320	27
GR23-19	Hochwipfel Fm		351389	5167790	686	302	27
GR23-20	Hochwipfel Fm	Mauthneralm Unit	359403	5165274	678	290	27
St14	Hochwipfel Fm	Mauthneralm Unit	358133	5163952	1272	283	27
Ob1	Nölbling Fm	Rauchkofel Imbricate	355222	5165467	1120	269	27
St1	Hochwipfel Fm	Rauchkofel Imbricate	355282	5162959	1758	264	27
St7	Auernig Fm	Stranig-Auernig Unit	356089	5162045	1733	261	27
St8	Auernig Fm	Stranig-Auernig Unit				270	27
Mauthen Section							
GR22-17	Meerbach Fm		346063	5169093	729	469	28
GR22-13	Hochwipfel Fm		345872	5168753	756	425	28
GR22-16	Hochwipfel Fm		344874	5168284	977	381	28
GR22-15	Uggwa-Fm		344400	5169182	1077	331	27
GR22-14	Uggwa-Fm		344574	5169097	1062	331	27
GR23-12	Hochwipfel Fm	Bischofalm Unit	342720	5164813	1283	270	27
GR22-11	Hochwipfel Fm	Bischofalm Unit	345792	5163362	1433	244	27
GR22-10	Hochwipfel Fm	Bischofalm Unit	344465	5163644	1401	245	31
GR23-11	Hochwipfel Fm	Cellon-Kellerwand Nappe	342380	5162999	1350	248	27
GR23-10	Hochwipfel Fm	Cellon-Kellerwand Nappe	343454	5162212	1140	260	27
C3	Rauchkofel Fm					227	28
C1	Cardiola Fm	Cellon-Kellerwand Nappe	342389	5163780	1499	232	28
C2	Kok Fm					260	27
C4	Uggwa-Fm					267	27

Table 1: Samples (coordinates in the UTM33 system) and RSCM temperature estimates (°C, median of 20 spot measurements), labeled according to Schönlaub (1985b, 1987, 1989).

Sample depth	Formation		Temp [°C]	+/-	D-STA	sd
91.5	Werfen Fm	Campill Mb	220	24	223.4	13.9
92.0	Werfen Fm	Campill Mb	232	24	210.2	19.6
127.4	Werfen Fm		191	24	236.5	9.6
134.5	Werfen Fm		175	24	242.5	6.2
151.4	Werfen Fm		194	24	235.3	10.0
152.8	Werfen Fm		186	24	238.3	8.7
154.0	Werfen Fm		185	26	238.5	11.7
164.6	Werfen Fm		217	24	225.3	13.5
182.0	Werfen Fm		203	24	231.5	7.2
183.6	Werfen Fm		189	28	237.4	17.4
185.8	Werfen Fm		216	24	225.5	8.0
189.2	Werfen Fm		202	24	232.1	6.0
193.0	Werfen Fm		231	24	217.6	9.1
211.8	Werfen Fm		175	24	242.3	6.1
216.2	Werfen Fm		204	24	231.2	5.2
220.4	Werfen Fm	Tesero Horizon	212	24	227.4	8.9
221.5	Werfen Fm	Tesero Horizon	203	24	231.7	7.7
229.4	Werfen Fm	Tesero Horizon	170	24	244.1	5.4
232.0	Bellerophon Fm		198	24	233.7	8.4
233.4	Bellerophon Fm		238	25	213.3	11.0
255.7	Bellerophon Fm		215	24	226.3	15.0
Sample name						
KL14_5A			162	30	236.5	7.7
KL14_21			228	30	224.7	7.1
KL14_16			236	30	228.2	9.1
KL16_31			236	30	211.8	7.6

Table 2: D-STA (total area, scaled by the D-band maximum intensity values (sd= standard deviation) and RSCM temperature estimates (°C) in the Gartnerkofel-1 core (median of 20 spot measurements) in comparison to four calibration samples (KL samples) of Lünsdorf et al. (2017).

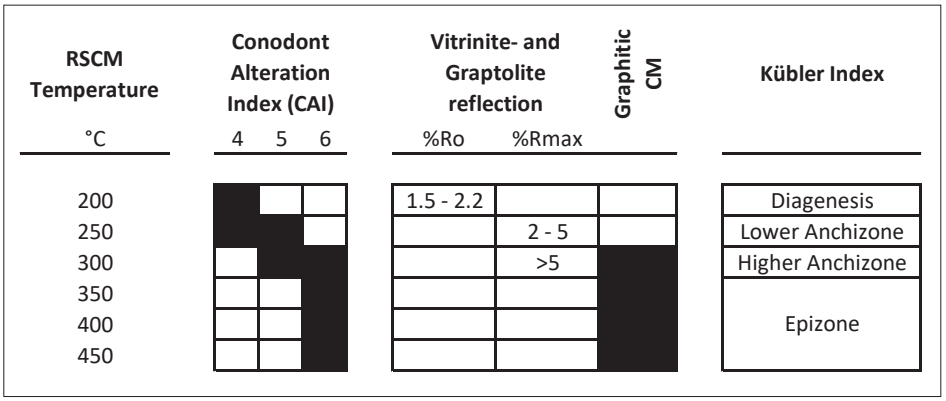

Table 3: Conodont Alteration Index data (Brime et al., 2008), graptolite- and vitrinite-reflectance values (Rantitsch, 1992; Sassi et al., 1995; Rantitsch, 1995b, 1997; Rantitsch et al., 2000; Rainer and Rantitsch, 2002; Rantitsch, 2007), and KI data (Árkai et al., 1991; Schramm, 1991; Schönlaub et al., 1992; Árkai et al., 1995; Sassi et al., 1995; Läufer et al., 1997; Rantitsch, 1997; Hubich et al., 2000; Nussbaum, 2000; Brime et al., 2008) correlated to RSCM temperatures of the Carnic Alps.

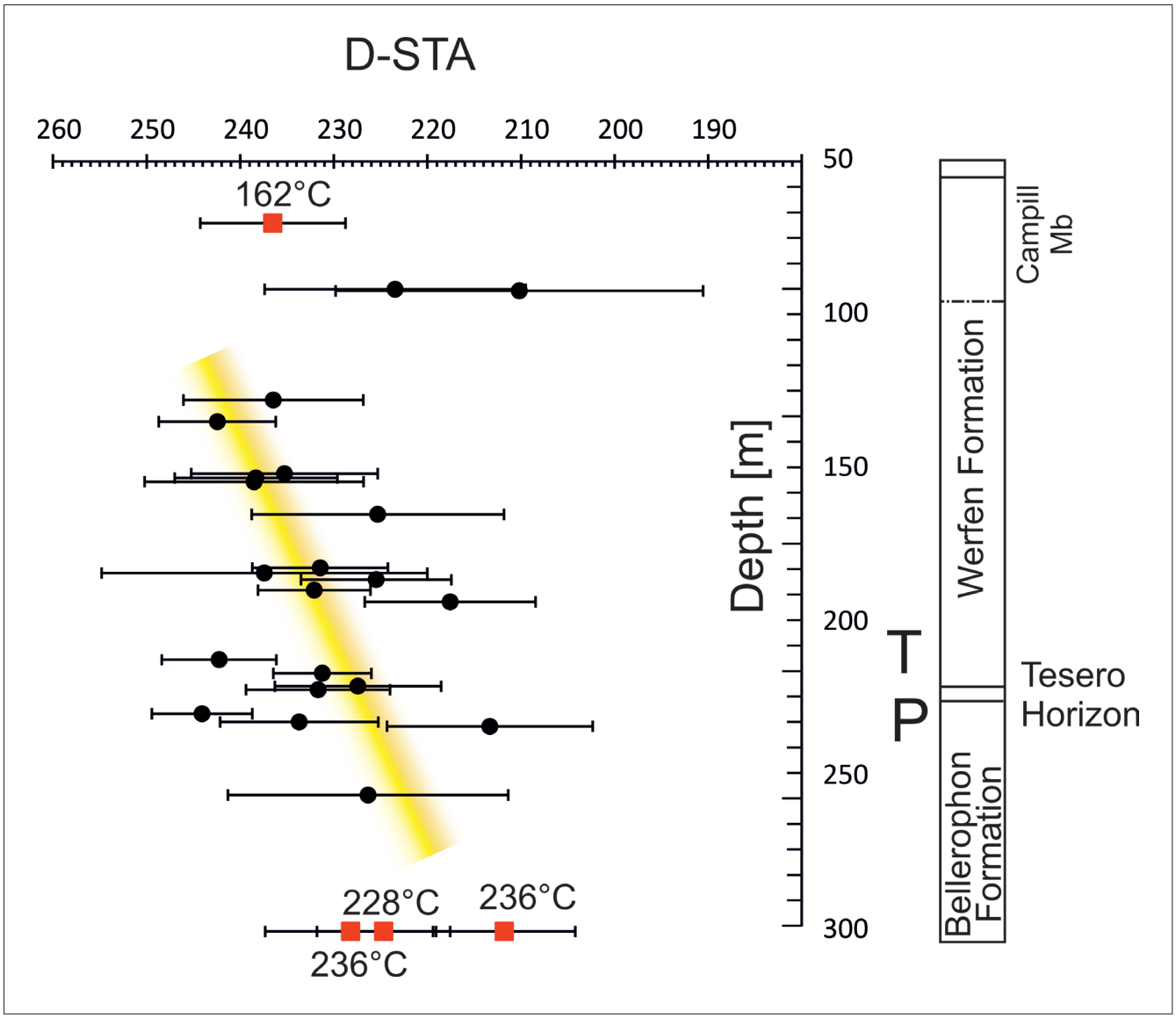

Figure 4: D-STA parameter (total area, scaled by the D-band maximum intensity; rising values indicate lower temperatures) of Lünsdorf et al. (2017) estimated on carbonaceous material of the Gartnerkofel-1 core (median and standard deviation) indicate a slight trend (yellow bar) to higher burial temperatures towards the bottom (stratigraphic data from Böckelmann, 1991). The RSCM temperatures are constrained by four standard samples (Tab. 2) of Lünsdorf et al. (2017) with well-established burial temperatures (red squares). Data far from the trendline are explained by a dominant detrital population within the sample. Pelites at the Permian-Triassic boundary (Tesero Horizon) were subjected to a burial temperature of ca. 200 °C (± 30 °C).

Schwarzwipfel Fault, samples from the bottom yield ca. 290 °C. In the Auernig Formation of the Stranig-Auernig Unit above, the temperature decreases to 261 °C. Lower temperatures between 229 °C and 247 °C are estimated from the Gartnerkofel Nappe, covering also the temperature range of the southern segment of the Stranig-Auernig Unit. No temperature hiatus occurs at the northern as well as the southern section segment between the syn-Variscan Hochwipfel Formation and the post-Variscan Auernig Formation.

CM ordering, as reflected by the D-STA parameter of Lünsdorf et al. (2017) indicate ca. 200 °C (± 30 °C) in the Permian-Triassic boundary sediments (Tesero Horizon) of the Gartnerkofel-1 core (Tab. 2, Fig. 4). The profile illustrates the within-sample scatter of the temperature indicator and the presence of detrital CM populations, in particular in samples from the base of the Campill Member of the Werfen Formation, corresponding to a significant proportion on terrigenous minerals in this section (Böckelmann, 1991). A slight offset of the D-STA values at the base of the Werfen Formation in the core interval between 193 and 212 m (Fig. 4) might be explained by a change in the microstructure of the plant debris, following the end Permian mass extinction (Benton and Newell, 2014).

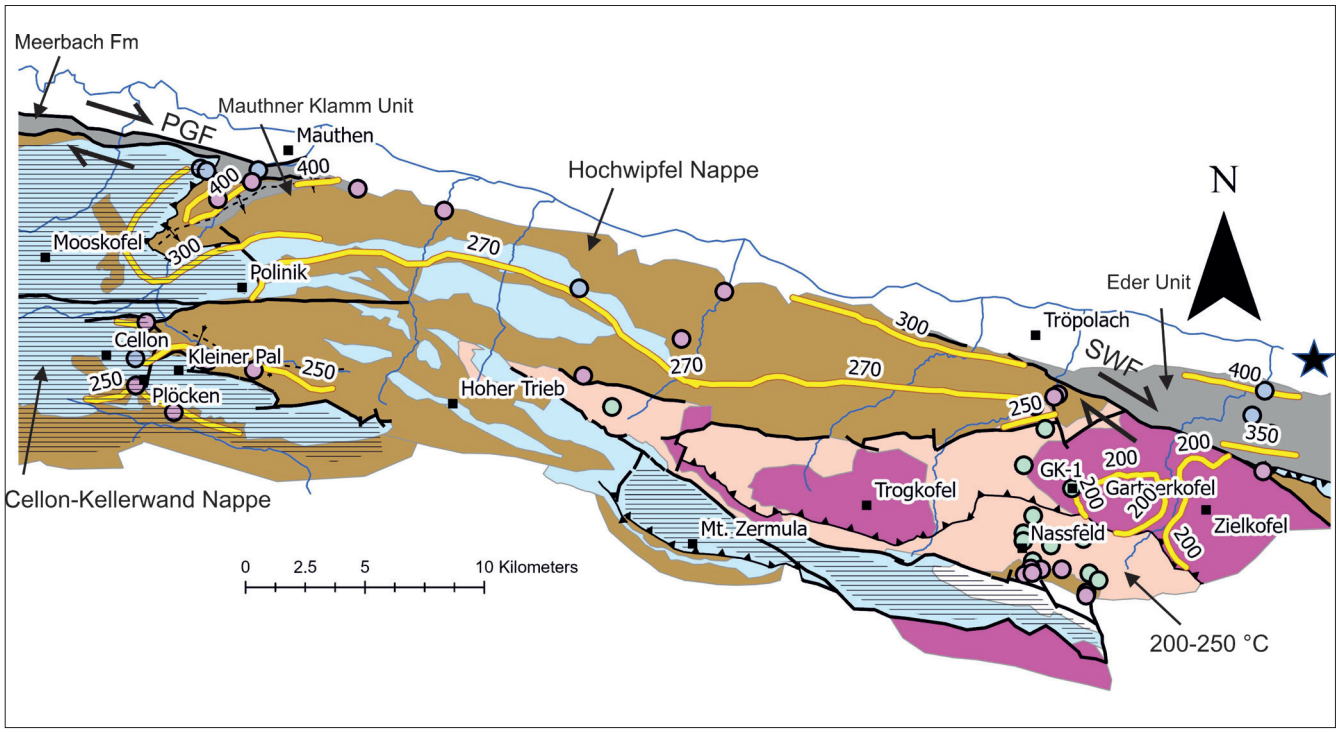

Figure 5: RSCM temperature (°C) isograde in the Carnic Alps (legend in Fig. 2). The 200 °C isotherm traces the formation boundary between the Werfen and Bellerophon Formations (not shown) as seen in the Gartnerkofel-1 core (Tab. 2, Fig. 4). The Meerbach Formation in the west of the study area is interpreted as a fault-bounded transpressionally exhumed block along the Pustertal-Gailtal Fault (PGF), structurally below the deepest segment of the Hochwipfel Nappe. The isotherm offset at the dextral Schwarzwipfel Fault (SWF) indicates a lateral displacement of more than 8 km. A black star indicates the presence of Periadriatic magmatics (Schönlaub, 1989).

6. Discussion

The obtained thermometric data constrain the tectono-stratigraphical upward trend of decreasing metamorphic temperatures (Fig. 5). Isotherms are constructed by using the RSCM data (Tabs. 1, 2) and correlated CAI values, graptolite and vitrinite reflectance values, as well as Kübler Index data (Tab. 3). Remarkably, the correlation between CAI and RSCM temperatures resembles the correlation established for Triassic conodonts (Rantitsch et al., 2020b).

The highest RSCM temperature of 469 °C (± 28 °C) identifies a small fault-bounded slice of mylonitic schists (Meerbach Formation of Schönlaub, 1985a, b) at the bottom of the Mauthen Section as the tectonically deepest unit of the Carnic Alps. The schists are mapped in a narrow zone along the Pustertal-Gailtal Fault (Schönlaub, 1985b, 1997), interpreted as a transpressionally exhumed block (Luggau Unit) by Läufer et al. (1997, 2001). A lower temperature range (425–320 °C) characterizes the adjacent part of the Mauthner Klamm Unit of Läufer et al. (2001 outcropping in a NE-SW-trending anticline (Schönlaub, 1985a, b). The data of this study demonstrate at the northwestern anticline limb an undisturbed metamorphic gradient of ca. 100 °C (331–425 °C, see Fig. 3a), crossing the footwall thrust of the Cellon-Kellerwand Nappe, in a vertical section of ca. 300 m thickness (Schönlaub, 1985b). The observation of undisturbed metamorphic isograde towards the hangingwall contradicts the model of a block, transpressionally exhumed below a lower metamorphic nappe-stack (Läufer et al., 1997, 2001). Thus, this segment is interpreted here as the deepest part of the Hochwipfel Nappe. The adjacent mylonitic schists in the north forms its former footwall, displaced laterally by dextral shearing along the Pustertal-Gailtal Fault (Läufer et al., 1997, 2001).

Separated by the dextral Schwarzwipfel Fault (Forke et al., 2008) from the Hochwipfel Nappe, the Eder Unit crops out at the eastern end of the study area (Schönlaub, 1989; Fig. 2). It was identified as a transpressionally exhumed unit and correlated to the Mauthner Klamm Unit by Läufer et al. (1997, 2001). The isotherm offset at the Schwarzwipfel Fault indicates a lateral component of the bulk displacement of more than 8 km. The internal metamorphic pattern (Fig. 5) and the missing metamorphic break towards the overlying Hochwipfel Nappe (Fig. 3b) resembles the observations in the Mauthen Section (see above). Thus, they are parts of the same structural level at the bottom of the Hochwipfel Nappe, displaced in the east (Nassfeld Section) by Oligocene dextral shearing along the Schwarzwipfel Fault (Läufer et al., 1997, 2001). Structural and geochronological data from the Eder Unit indicate subhorizontal dextral shearing during this time, followed by Miocene exhumation (Läufer et al., 1997, 2001). In the view of the presented metamorphic

data, this implies ductile shearing at the northern edge of the Hochwipfel Nappe during the Oligocene and a subsequent exhumation of the entire Carnic Alps during the Miocene, not only preserved in some isolated blocks adjacent to the Periadriatic Fault System.

In map view it is notable to see a very dense local isotherm pattern at the base of the Mauthen Section (Fig. 5). As the rocks within this zone have been highly strained (Läufer et al., 1997), an increase of CM lattice ordering due to frictional shearing (Barzoi, 2015; Cao and Neubauer, 2019; Kedar et al., 2020) must be considered, as crystal-plasticity temperatures of ductily deformed minerals (Läufer et al., 1997) are here in the range of the RSCM temperatures. However, the temperature pattern in the Mauthen Section (Figs. 3a, 5) indicates that strain-induced lattice-ordering was of minor importance. The stratigraphic upward increase of the paleotemperatures suggests a local heat pulse at the base of the section, affecting the area outlined by the 400 °C isotherm (Fig. 5). In the Mauthen Section, the isotherms crosscut an anticline of uncertain age. However, an Oligocene age of this structure is suggested by reference to the paleostress data of Bartel et al. (2014). Consequently, in accordance to age data of Läufer et al. (1997), metamorphism after folding might be indicated. Subsequently, progressive exhumation since the Miocene may have exposed the core of the anticline to the surface. Oligocene magmatic rocks occur adjacent to the Eder Unit of the Nassfeld Section (Schönlaub and Exner, 1984; Schönlaub, 1989; Fig. 5) and west of the Mauthen Section (Exner, 1976; Sprenger, 1996; Schönlaub, 1997). Thus, they may have provided the heat-source for a local contact metamorphic overprint, locally also causing anomalously high CAI values in conodonts from the Mauthen Section (Brime et al., 2008). Klotz et al. (2019) described a similar effect by a reset of zircon fission track ages close to a large Oligocene intrusion along the Peridriatic Fault System reaching up to a distance of ca. 300 m.

Metamorphic temperatures in the Hochwipfel Nappe decrease continuously to ca. 250 °C. The metamorphic isotherms follow the Variscan imbrication pattern. As observed in three locations, post-Variscan sediments overly the Hochwipfel Nappe without a metamorphic break. Boundary temperatures decrease from 260 °C in the west and north to ca. 230 °C in the southeast. This gradient is also present in a west-to-east decrease of CAI values in Devonian carbonates south of the Nassfeld area (Brime et al., 2008). According to a numerical thermal model (Rantitsch, 1997), this is explained by a variation of the Permo-Mesozoic burial depths. Thus, the Hochwipfel Nappe exposes a temperature gradient between ca. 250 and 320 °C outside the overprinted area (see above; Fig. 3) which is correlated to an approximated maximum thickness of the Hochwipfel Formation of ca. 1 km (Corradini and Suttner, 2015). Jirman et al. (2018) provided a thermal model of an age-equivalent flysch basin (Jesenik Basin of the Moravian-Silesian Belt), paleogeographically situated in a more internal position of the Variscan chain. The thermal maturity (i.e., vitrinite reflectance) of this basin resembles the maturity range of the Hochwipfel flysch. In the Jesenik Basin, a thickness of up to 7.3 km of overburden on top of the exposed flysch sequence explains a burial temperature of 310–395 °C in a depth interval of ca. 3 km. In comparison, the sediments of the Hochwipfel Nappe must have been obviously heated at a heat flow significantly exceeding the "normal" heat flow (63 mW/m^2) estimated for the Moravian-Silesian Belt (Jirman et al., 2018). This is supported by clay mineralogical data (Sassi et al., 1995; Rantitsch, 1997) and thermal modeling (Rantitsch, 1997) and was attributed to an increased post-Variscan heat-flow during post-Variscan times (Rantitsch, 1997; Rantitsch et al., 2020a).

The Cellon Section of the Cellon-Kellerwand Nappe at the top of the Mauthen Section exposes in a fragmented Variscan anticline an upward decreasing thermal gradient in Ordovician-Silurian strata. Pennsylvanian flysch sediments at the top (exposed in the south and in a syncline north of the mountain crest) show 244–270 °C. In map view it is obvious that isotherms cross-cut the fold pattern, but decrease with increasing altitude (Tab. 1, Fig. 5), indicating Permo-Mesozoic burial heating, constrained also by RSCM temperatures estimated for Permian-Triassic boundary sediments in the Gartnerkofel-1 core (Fig. 4). They indicate a temperature difference of ca. 50 °C within a stratigraphical interval of ca. 1.5 km thickness (Schönlaub and Forke, 2007). This gradient is significantly lower than the gradient estimated for the Hochwipfel Nappe, thus indicating a lower heat-flow during post-Permian burial.

7. Conclusions

RSCM temperatures refine the view on the metamorphic structure of the central and eastern Carnic Alps. Although there is no metamorphic break at the Variscan unconformity, RSCM temperatures discriminate Variscan and Alpine metamorphic processes of a similar grade. The pattern of metamorphic isotherms identifies three domains of different tectono-metamorphic histories: (1) In the central Carnic Alps (south of Mauthen), a fault-bounded and dextral-transpressionally placed block, adjacent to the Periadriatic Fault System, is characterized by the highest temperature estimate (469 °C). Without a break, a dense pattern of upward decreasing RSCM isotherms is observed in the Mauthner Klamm area. The Eder Unit of the eastern Carnic Alps shows the same metamorphic imprint. Because of a missing metamorphic break towards the hangingwall, both units are interpreted as deepest segments of the Hochwipfel Nappe. (2) The upper part of the Hochwipfel Nappe is characterized by structurally controlled isotherms, indicating a high thermal gradient (ca. 70 °C/km) of presumably Variscan age. (3) Isotherms of the Cellon-Kellerwand Nappe at the top cross-cut Variscan folds, thus indicating post-Variscan heating under a lower thermal gradient (ca. 30 °C/km) as observed in Pennsylvanian to Lower Triassic sediments.

The reconstructed metamorphic history comprises Variscan burial of an accretionary wedge (preserved in the Hochwipfel Nappe), burial below Permo-Mesozoic cover sequences (preserved in the Cellon-Kellerwand Nappe and in the post-Variscan cover units), and presumable Oligocene contact metamorphism of the tectonically deepest units of the Hochwipfel Nappe (preserved in the Mauthner Klamm area and in the Eder Unit).

Acknowledgement

Bianca Heberer, Istvan Dunkl, and an anonymous reviewer are thanked for helpful comments. Hugo Ortner and Kurt Stüwe are thanked for the careful editorial handling and comments.

References

Árkai, P., Sassi, R., Zirpoli, G., 1991. On the boundary between the low- and very low-grade South-Alpine basement in Pustertal: X-ray characterization of white mica in metapelites between Dobbiaco (Toblach, Italy) and Leiten (Austria) (Eastern Alps). Memorie di scienze geologiche, 43, 293–304.

Árkai, P., Sassi, F.P., Sassi, R., 1995. Simultaneous measurements of chlorite and illite crystallinity: a more reliable tool for monitoring low- to very low grade metamorphisms in metapelites. A case study from the Southern Alps (NE Italy). European Journal of Mineralogy, 7, 1115–1128.

Árkai, P., Livi, K.J., Frey, M., Brukner-Wein, A., Sajgó, C. de, 2004. White micas with mixed interlayer occupancy: a possible cause of pitfalls in applying illite Kubler index ("crystallinity") for the determination of metamorphic grade. European Journal of Mineralogy, 16, 469–482. https://doi.org/10.1127/0935-1221/2004/0016-0469.

Bartel, E.M., Neubauer, F., Genser, J., Heberer, B., 2014. States of paleostress north and south of the Periadriatic fault: Comparison of the Drau Range and the Friuli Southalpine wedge. Tectonophysics, 637, 305–327. https://doi.org/10.1016/j.tecto.2014.10.019

Barzoi, S.C., 2015. Shear stress in the graphitization of carbonaceous matter during the low-grade metamorphism from the northern Parang Mountains (South Carpathians) – Implications to graphite geothermometry. International Journal of Coal Geology. 146, 179–187. https://doi.org/10.1016/j.coal.2015.05.008.

Benton, M.J., Newell, A.J., 2014. Impacts of global warming on Permo-Triassic terrestrial ecosystems. Gondwana Research. 25, 1308–1337. https://doi.org/10.1016/j.gr.2012.12.010.

Böckelmann, K., 1991. The Permian-Triassic of the Gartnerkofel-1 core and the Reppwand Section (Carnic Alps, Austria). Abhandlungen der geologischen Bundesanstalt, 45, 17–36.

Brime, C., Perri, M.C., Pondrelli, M., Spalletta, C., Venturini, C., 2008. Polyphase metamorphism in the eastern Carnic Alps (N Italy-S Austria). International Journal of Earth Sciences, 97, 1213–1229. https://doi.org/10.1007/s00531-007-0218-7

Cao, S., Neubauer, F., 2019. Graphitic material in fault zones: Implications for fault strength and carbon cycle. Earth-Science Reviews, 194, 109–124. https://doi.org/10.1016/j.earscirev.2019.05.008

Castellarin, A., Cantelli, L., 2000. Neo-Alpine evolution of the Southern Eastern Alps. Journal of Geodynamics, 30, 251–274. https://doi.org/10.1016/S0264-3707(99)00036-8

Corradini, C., Suttner, T. (eds.), 2015. The pre-Variscan sequence of the Carnic Alps (Austria and Italy). Abhandlungen der Geologischen Bundesanstalt, 69, 1–158.

Corradini, C., Corriga, M.G., Männik, P., Schönlaub, H.P., 2015. Revised conodont stratigraphy of the Cellon section (Silurian, Carnic Alps). Lethaia, 48, 56–71. https://doi.org/10.1111/let.12087

Curzi, M., Viola, G., Zuccari, C., Aldega, L., Billi, A., van der Lelij, R., Kylander-Clark, A., Vignaroli, G., 2024. Tectonic Evolution of the Eastern Southern Alps (Italy): A Reappraisal from new structural data and geochronological constraints. Tectonics. 43/3. https://doi.org/10.1029/2023TC008013

Dallmeyer, R.D., Neubauer, F., 1994. Cadomian 40Ar/39Ar apparent age spectra of detrital muscovite from the Eastern Alps. Journal of the Geological Society, 151, 591–598.

Ebner, F., Vozárová, A., Kovács, S., Kräutner, H.-G., Krstić, B., Szederkenyi, T., Jamicic, D., Balen, D., Belak, M., Trajanova, M., 2008. Devonian – Carboniferous pre-flysch and flysch environments in the Circum Pannonian Region. Geologica Carpathica, 59, 159–195.

Epstein, A.G., Epstein, J.B., Harris, L.D., 1977. Conodont Color Alteration-an index to organic metamorphism. Geological Survey Professional paper, 995, 1–26.

Exner, C., 1976. Die geologische Position der Magmatite des periadriatischen Lineamentes. Verhandlungen der Geologischen Bundesanstalt, 1976, 3–64.

Ferreiro Mählmann, R., Bozkaya, Ö., Potel, S., Le Bayon, R., Šegvić, B., Nieto, F., 2012. The pioneer work of Bernard Kübler and Martin Frey in very low-grade metamorphic terranes: paleo-geothermal potential of variation in Kübler-Index/organic matter reflectance correlations. A review. Swiss Journal of Geosciences, 105, 121–152. https://doi.org/10.1007/s00015-012-0115-3

Fodor, L., Jelen, B., Márton, E., Skaberne, D., Car, J., Vrabec, M., 1998. Miocene-Pliocene tectonic evolution of the Slovenian Periadriatic fault: Implications for Alpine-Carpathian extrusion models. Tectonics, 17, 690–709.

Forke, H., Novak, M., Vrabec, M., 2008. Implication of facies relationships of Upper Carboniferous/Lower Permian sediments in the Southern Alps (Carnic Alps/Karavanke Mts.) for Late Paleozoic paleogeography and Neogene tectonics. Journal of Alpine Geology, 49, 25.

Frisch, W., Kuhlemann, J., Dunkl, I., Brügel, A., 1998. Palinspastic reconstruction and topographic evolution of the Eastern Alps during late Tertiary tectonic extrusion. Tectonophysics, 297, 1–15. https://doi.org/ 10.1016/S0040-1951(98)00160-7

Frisch, W., Dunkl, I., Kuhlemann, J., 2000. Post-collisional orogen-parallel large-scale extension in the Eastern Alps. Tectonophysics, 327/3–4, 239–265. https://doi.org/10.1016/S0040-1951(00)00204-3

Haas, I., Eichinger, S., Haller, D., Fritz, H., Nievoll, J., Mandl, M., Hippler, D., Hauzenberger, C., 2020. Gondwana fragments in the Eastern Alps: A travel story from U/Pb zircon data. Gondwana Research, 77, 204–222. https://doi.org/10.1016/j.gr.2019.07.015

Heberer, B., Reverman, R.L., Fellin, M. G., Neubauer, F., Dunkl, I., Zattin, M., Seward, D., Genser, J., Brack, P., 2017. Postcollisional cooling history of the Eastern and Southern Alps and its linkage to Adria indentation. International Journal of Earth Sciences, 106, 1557–1580. https://doi.org/10.1007/s00531-016-1367-3

Henry, D.G., Jarvis, I., Gillmore, G., Stephenson, M., 2019. Raman spectroscopy as a tool to determine the thermal maturity of organic matter: Application to sedimentary, metamorphic and structural geology. Earth-Science Reviews, 102936. https://doi.org/10.1016/j.earscirev.2019.102936

Holser, W.T., Schönlaub, H.P., 1991 (eds.). The Permian-Triassic boundary in the Carnic Alps of Austria (Gartnerkofel region). Abhandlungen der Geologischen Bundesanstalt, 45,1–232.

Holser, W.T., Schönlaub, H.-P., Attrep Jr., M., Boeckelmann, K., Klein, P., Magaritz, M., Orth, C.J., Fenninger, A., Jenny, C., Kralik, M., Mauritsch, H., Pak, E., Schramm, J.-M., Stattegger, K., Schmöller, R., 1989. A unique geochemical record at the Permian/Triassic boundary. Nature. 337, 39–44. https://doi.org/10.1038/337039a0.

Hubich, D., Läufer, A., Loeschke, J., Schrauder, A., Staiger, M., 2000. The boundary between the western and central Carnic Alps (Austria-Italy). Memorie de Science Geologiche, 52, 293–318.

Jaeger, H., Schönlaub, H.P., 1980. Silur und Devon nördlich der Gundersheimer Alm in den Karnischen Alpen (Osterreich). Carinthia II, 170/90, 403–444.

Jirman, P., Geršlová, E., Kalvoda, J., Melichar, R., 2018. 2D basin modelling in the eastern Variscan fold belt (Czech Republic): Influence of thrusting on patterns of thermal maturation. Journal of Petroleum Geology, 41, 175–188. https://doi.org/10.1111/jpg.12699.

Kedar, L., Bond, C.E., Muirhead, D., 2020. Carbon ordering in an aseismic shear zone: Implications for Raman geothermometry and strain tracking. Earth and Planetary Science Letters. 549, 116536. https://doi.org/10.1016/j.epsl.2020.116536.

Klotz, T., Pomella, H., Reiser, M., Fügenschuh, B., Zattin, M., 2019. Differential uplift on the boundary between the Eastern and the Southern European Alps: Thermochronologic constraints from the Brenner Base Tunnel. Terra Nova, 31, 281–294. https://doi.org/10.1111/ter.12398

Krainer, K., 1992. Fazies, Sedimentationsprozesse und Paläogeographie im Karbon der Ost- und Südalpen. Jahrbuch der Geologischen Bundesanstalt, 135, 99–193.

Kullmann, J., Loeschke, J., 1994. Olistholithe in Flysch-Sedimenten der Karawanken: Die Entwicklung eines aktiven Kontinentrandes im Karbon der Südalpen (Paläozoikum von Seeberg und Eisenkappel/Österreich). Neues Jahrbuch für Geologie und Paläontologie Abhandlungen, 194, 115–142.

Läufer, A.L., 1996. Variscan and Alpine tectonometamorphic evolution of the Carnic Alps (Southern Alps) – structural analysis, illite crystallinity, K-Ar and Ar-Ar geochronology. Tübinger Geowissenschaftliche Arbeiten, Reihe A, 26, 1–102.

Läufer, A.L., Loeschke, J., Vianden, B., 1993. Die Dimon-Serie der Karnischen Alpen (Italien) – Stratigraphie, Petrographie und geodynarnische Interpretation. Jahrbuch der Geologischen Bundesanstalt, 136, 137–162.

Läufer, A.L., Frisch, W., Steinitz, G., Loeschke, J., 1997. Exhumed fault-bounded Alpine blocks along the Periadriatic lineament: the Eder unit (Carnic Alps, Austria). Geologische Rundschau, 86, 612–626. https://doi.org/10.1007/s005310050167

Läufer, A.L., Hubich, D., Loeschke, J., 2001. Variscan geodynamic evolution of the Carnic Alps (Austria/Italy). International Journal of Earth Sciences, 90, 855–870. https://doi.org/10.1007/s005310100194

Lünsdorf, N.K., 2016. Raman spectroscopy of dispersed vitrinite – Methodical aspects and correlation with reflectance. International Journal of Coal Geology, 153, 75–86. https://doi.org/10.1016/j.coal.2015.11.010

Lünsdorf, N.K., Lünsdorf, J.O., 2016. Evaluating Raman spectra of carbonaceous matter by automated, iterative curve-fitting. International Journal of Coal Geology, 160–161, 51–62. https://doi.org/10.1016/j.coal.2016.04.008

Lünsdorf, N.K., Dunkl, I., Schmidt, B.C., Rantitsch, G., Eynatten, H. von, 2014. Towards a higher comparability of geothermometric data obtained by Raman spectroscopy of carbonaceous material. Part I: Evaluation of biasing factors. Geostandards and Geoanalytical Research, 38, 73–94. https://doi.org/ 10.1111/j.1751-908X.2013.12011.x

Lünsdorf, N.K., Dunkl, I., Schmidt, B.C., Rantitsch, G., Eynatten, H. von, 2017. Towards a higher comparability of geothermometric data obtained by Raman spectroscopy of carbonaceous material. Part 2: A revised geothermometer. Geostandards and Geoanalytical Research, 41, 593–612. https://doi.org/10.1111/ggr.12178

McMillan, R., Golding, M., 2019. Thermal maturity of carbonaceous material in conodonts and the Color Alteration Index: Independently identifying maximum temperature with Raman spectroscopy. Palaeogeography, Palaeoclimatology, Palaeoecology, 534, 109290. https://doi.org/10.1016/j.palaeo.2019.109290

Mader, D., Neubauer, F., Handler, R., 2007. 40Ar/39Ar dating of detrital white mica of Upper Paleozoic sandstones in the Carnic Alps (Austria): Implications for provenance and tectonic setting. Geologica Carpathica, 58, 133–144.

Mancktelow, N., Stöckli, D., Grollimund, B., Müller, W., Fügenschuh, B., Viola, G., Seward, D., Villa, I., 2001. The DAV and Periadriatic fault systems in the Eastern Alps south of the Tauern window. International Journal of Earth Sciences, 90, 593–622. https://doi.org/10.1007/s005310000190

Mariotto, F.P., Venturini, C., 2019. Birth and evolution of the Paleocarnic Chain in the Southern Alps: a review. International Journal of Earth Sciences, 108, 2469–2492. https://doi.org/10.1007/s00531-019-01774-y

Meli, S., 2004. Rb-Sr and 40Ar/39Ar age constraints on the Variscan metamorphism recorded by Ordovician acidic metavolcanic rocks in the Eastern Southalpine basement. Rendiconti Lincei, 15, 205–223. https://doi.org/10.1007/BF02904461

Neubauer, F., Liu, Y., Dong, Y., Chang, R., Genser, J., Yuan, S., 2022. Pre-Alpine tectonic evolution of the Eastern Alps: From Prototethys to Paleotethys. Earth-Science Reviews, 226, 103923. https://doi.org/10.1016/j.earscirev.2022.103923

Nussbaum, C., 2000. Neogene tectonics and thermal maturity of sediments of the easternmost Southern Alps (Friuli area, Italy). PhD thesis, Université de Neuchâtel, 160 pp.

Pondrelli, M., 2002. Thermal history of the Carnic Alps (NE Italy-S. Austria) using CAI analysis. Revista Italiana di Paleontologia e Stratigrafia, 108, 369–380. https://doi.org/10.13130/2039-4942/5482

Pondrelli, M., Corradini, C., Spalletta, C., Simonetto, L., Perri, M.C., Corriga, M.G., Venturini, C., Schönlaub, H.P., 2020. Geological map and stratigraphic evolution of the central sector of the Carnic Alps (Austria-Italy). Italian Journal of Geosciences, 139, 469–484. https://doi.org/10.3301/IJG.2020.16

Pusz, S., Borrego, A.G., Alvarez, D., Camean, I., Du Cann, V., Duber, S., Kalkreuth, W., Komorek, J., Kus, J., Kwiecińska, B.K., Libera, M., Marques, M., Misz-Kennan, M., Morga, R., Rodrigues, S., Smędowski, Ł., Suarez-Ruiz, I., Strzezik, J., 2014. Application of reflectance parameters in the estimation of the structural order of coals and carbonaceous materials. Precision and bias of measurements derived from the ICCP structural working group. International Journal of Coal Geology, 131, 147–161. https://doi.org/10.1016/j.coal.2014.04.004

Rainer, T., Rantitsch, G., 2002. Vitrinitreflexion im Bohrkern Gartnerkofel-1 (Perm bis Skyth, Karnische Alpen, Kärnten). Carinthia II, 192, 449–454.

Rainer, T., Sachsenhofer, R.F., Rantitsch, G., Herlec, U., Vrabec, M., 2009. Organic maturity trends across the Variscan discordance in the Alpine-Dinaric Transition Zone (Slovenia, Austria, Italy): Variscan versus Alpidic thermal overprint. Austrian Journal of Earth Sciences, 102, 120–133.

Rainer, T., Sachsenhofer, R.F., Green, P.F., Rantitsch, G., Herlec, U., Vrabec, M., 2016. Thermal maturity of Carboniferous to Eocene Sediments of the Alpine-Dinaric Transition Zone (Slovenia). International Journal of Coal Geology, 157, 19–38. https://doi.org/10.1016/j.coal.2015.08.005

Rantitsch, G., 1992. Reflexionsmessungen an Graptolithen im Silur und Unterdevon der Karnischen Alpen (Österreich). Jahrbuch der Geologischen Bundesanstalt, 135, 299–316.

Rantitsch, G., 1995a. Niedrigstgradige Metamorphose im Karbon von Nötsch (Österreich). Jahrbuch der Geologischen Bundesanstalt., 138, 433–440.

Rantitsch, G., 1995b. Coalification and graphitization of graptolites in the anchizone and lower epizone. International Journal of Coal Geology, 27, 1–22. https://doi.org/10.1016/0166-5162(94)00017-T

Rantitsch, G., 1997. Thermal history of the Carnic Alps (Southern Alps, Austria) and its palaeogeographic implications. Tectonophysics, 272, 213–232. https://doi.org/10.1016/S0040-1951(96)00259-4

Rantitsch, G., 2007. Organische Metamorphose am Auernig (Naßfeld, Karnische Alpen). Jahrbuch der Geologischen Bundesanstalt, 147, 331–334.

Rantitsch, G., 2023. Graphite thermometry by interactive fitting of Raman spectra. International Journal of Coal Geology, 271, 104232. https://doi.org/10.1016/j.coal.2023.104232

Rantitsch, G., Rainer, T., 2003. Thermal modeling of Carboniferous to Triassic sediments of the Karawanken Range (Southern Alps) as a tool for paleogeographic reconstructions in the Alpine-Dinaridic-Pannonian realm, International Journal of Earth Sciences, 92, 195–209. https://doi.org/10.1007/s00531-003-0312-4

Rantitsch, G., Rainer, T., Russegger, B., 2000. Niedrigstgradige Metamorphose im Karbon der Südalpen (Kärnten, Österreich). Carinthia II, 190, 537–542.

Rantitsch, G., Iglseder, C., Schuster, R., Hollinetz, M.S., Huet, B., Werdenich, M., 2020a. Organic metamorphism as a key for reconstructing tectonic processes: a case study from the Austroalpine unit (Eastern Alps). International Journal of Earth Sciences, 109, 2235–2253. https://doi.org/10.1007/s00531-020-01897-7

Rantitsch, G., Bryda, G., Gawlick, H.-J., 2020b. Conodont thermometry

by Raman spectroscopy on carbonaceous material: a case study from the Northern Calcareous Alps (Mürzalpen Nappe, Eastern Alps). Austrian Journal of Earth Sciences. 113, 201–210. https://doi.org/10.17738/ajes.2020.0012.

Rejebian, V.A., Harris, A.G., Huebner, J.S., 1987. Conodont color and textural alteration: An index to regional metamorphism, contact metamorphism, and hydrothermal alteration. Geological Society of America Bulletin, 99, 471–479.

Sassi, R., Árkai, P., Lantai, C., Venturini, C., 1995. Location of the boundary between the metamorphic Southalpine basement and the Paleozoic sequences of the Carnic Alps – illite crystallinity and vitrinite reflectance data. Schweizerische Mineralogische und Petrographische Mitteilungen, 75, 399–412.

Sassi, R., Venturini, C., Árkai, P., 2004. The boundary between the metamorphic and nonto anchi-metamorphic domains in the Southalpine basement s.l. of the eastern southern Alps: a review. Periodico di Mineralogia. 73, 131–143.

Schmid, S.M., Fügenschuh, B., Kissling, E., Schuster, R., 2004. Tectonic map and overall architecture of the Alpine orogen. Eclogae Geologicae Helvetiae, 97, 93–117. https://doi.org/10.1007/s00015-004-1113-x

Schönlaub, H.P., 1985a. Das Paläozoikum der Karnischen Alpen. Arbeitstagung der Geologischen Bundesanstalt 1985, Kötschach-Mauthen, 34–52.

Schönlaub, H.P. (ed.), 1985 b. Geologische Karte der Republik Österreich 1:50 000. 197 Kötschach. Geologische Bundesanstalt, Wien.

Schönlaub, H.P. (ed.), 1987. Geologische Karte der Republik Österreich 1:50 000. 198 Weissbriach. Geologische Bundesanstalt, Wien.

Schönlaub, H.P. (ed.), 1989. Geologische Karte der Republik Österreich 1:50 000. 199 Hermagor. Geologische Bundesanstalt, Wien.

Schönlaub, H.P. (ed.), 1997. Geologische Karte der Republik Österreich 1:50 000. 196 Obertilliach. Geologische Bundesanstalt, Wien.

Schönlaub, H.P. (ed.), 2007. Geologischen Karte des Jungpaläozoikums der Karnischen Alpen 1:12 500. Geologische Bundesanstalt, Wien.

Schönlaub, H.P., Exner, C., 1984. Ein neues Vorkommen von Tonalitgneis und Gailtalkristallin im mittleren Gailtal. Jahrbuch der Geologischen Bundesanstalt, 127, 181–186.

Schönlaub, H.P., Forke, H.C., 2007. Die post-variszische Schichtfolge der Karnischen Alpen – Erläuterungen zur Geologischen Karte des Jungpaläozoikums der Karnischen Alpen 1:12 500. Abhandlungen der Geologischen Bundesanstalt, 61, 3–157.

Schönlaub, H.P., Forke, H., 2023. Das geologische Erbe der Karnischen Alpen. Naturwissenschaftlicher Verein für Kärnten. Klagenfurt, 304 pp.

Schönlaub, H.P., Heinisch, H., 1993. The classic fossiliferous Palaeozoic units of the Eastern and Southern Alps. In: Raumer, J.F. von, Neubauer, F. (eds.) Pre-Mesozoic geology in the Alps. Springer-Verlag, Berlin, 395–422.

Schönlaub, H.P., Histon, K., 2000. The Palaeozoic evolution of the Southern Alps. Mitteilungen der österreichischen geologischen Gesellschaft, 92, 15–34.

Schönlaub, H.P., Attrep, M., Boeckelmann, K., Dreesen, Roland J.M.J., Feist, R., Fenninger, A., Hahn, G., Klein, P., Korn, D., Kratz, R., Magaritz, M., Orth, C.J., Schramm, J.-M., 1992. The Devonian/Carboniferous boundary in the Carnic Alps (Austria) – A multidisciplinary approach. Jahrbuch der Geologischen Bundesanstalt, 135, 57–98.

Schramm, J.M., 1991. The Permian-Triassic of the Gartnerkofel-1 core (Carnic Alps, Austria): Illite Crystallinity in shaly sediments and its comparison with pre-Variscan sequences. Abhandlungen der Geologischen Bundesanstalt, 45, 69–77.

Siegesmund, S., Oriolo, S., Broge, A., Hueck, M., Lammerer, B., Basei, M.A.S., Schulz, B., 2023. Cadomian to Cenerian accretionary orogenic processes in the Alpine basement: the detrital zircon archive. International Journal of Earth Sciences, https://doi.org/10.1007/s00531-023-02305-6

Sprenger, W.L., 1996. Das Periadriatische Lineament südlich der Lienzer Dolomiten. Strukturgeologie – Fernerkundung – Geochemie. Abhandlungen der Geologischen Bundesanstalt, 52, 1–220.

Venturini, C., Pondrelli, M., Fontana, C., Delzotto, S., Discenza, K., 2001. Carta geologica delle Alpi Carniche. 1:25 000, Società elaborazioni cartografiche, Firenze.

Vrabec, M., Fodor, L., 2006. Late Cenozoic tectonics of Slovenia: Structural styles at the northeastern corner of the Adriatic Microplate. In: Pinter, N., Gyula, G., Weber, J., Stein, S., Medak, D. (eds.), The Adria Microplate: GPS Geodesy, Tectonics and Hazards. Springer, Berlin, 151-168. https://doi.org/10.1007/1-4020-4235-3_10

Warr, L.N., Ferreiro Mählmann, R., 2015. Recommendations for Kübler Index standardization. Clay Minerals, 50, 283–286. https://doi.org/10.1180/claymin.2015.050.3.02

Received: 14.2.2024
Accepted: 26.4.2024
Editorial Handling: Hugo Ortner